

See discussions, stats, and author profiles for this publication at: <https://www.researchgate.net/publication/228533005>

Three-dimensional localization of *in vivo* bioluminescent source based on multispectral imaging

Article *in* Proceedings of SPIE - The International Society for Optical Engineering · February 2009

DOI: 10.1117/12.811329

CITATIONS

0

READS

16

5 authors, including:



Jinchao Feng

Beijing University of Technology

34 PUBLICATIONS 355 CITATIONS

[SEE PROFILE](#)



Jie Tian

Chinese Academy of Sciences

661 PUBLICATIONS 7,114 CITATIONS

[SEE PROFILE](#)



Shuping Zhu

Xidian University

49 PUBLICATIONS 629 CITATIONS

[SEE PROFILE](#)

All content following this page was uploaded by [Jie Tian](#) on 12 October 2015.

The user has requested enhancement of the downloaded file. All in-text references [underlined in blue](#) are added to the original document and are linked to publications on ResearchGate, letting you access and read them immediately.

Three-dimensional localization of *in vivo* bioluminescent source based on multispectral imaging

Jinchao Feng^a, Kebin Jia^a, Jie Tian^{b,c}, Guorui Yan^b and Shouping Zhu^b

^aThe College of Electronic Information & Control Engineering, Beijing University of Technology, Beijing 100022, China

^bMedical Image Processing Group, Key Laboratory of Complex Systems and Intelligence Science, Institute of Automation, Chinese Academy of Sciences, P. O. Box 2728, Beijing 100190, China

^cLife Science Research Center, Xidian University, Xi'an 710071, China

ABSTRACT

Bioluminescence tomography (BLT) is a novel *in vivo* technique in small animal studies, which can reveal the molecular and cellular information at the whole-body small animal level. At present, there is an increasing interest in multispectral bioluminescence tomography, since multispectral data acquisition could improve the BLT performance significantly. In view to the ill-posedness of BLT problem, we develop an optimal permissible source region strategy to constrain the possible solution of the source by utilizing spectrum character of bioluminescent source. Then a linear system to link the measured data with the unknown light source variables is established by utilizing the optimal permissible region strategy based on adaptive finite element analysis. Furthermore, singular value decomposition analysis is used for data dimensionality reduction and improving computational efficiency in multispectral case. The reconstructed speed and stability benefit from adaptive finite element, the permissible region strategy and singular value decomposition. In the numerical simulation, the heterogeneous phantom experiment has been used to evaluate the performance of the proposed algorithm with the Monte Carlo based synthetic data. The reconstruction results demonstrate the merits and potential of our methodology for localizing bioluminescent source.

Keywords: multispectral bioluminescence tomography (BLT), optimal permissible source region, diffusion approximation, adaptive finite element method, singular value decomposition analysis, Monte Carlo methods

1. INTRODUCTION

Small animal imaging is increasingly being used as an important tools to reveal the molecular and cellular information *in vivo*.¹ To study a small animal with molecular imaging techniques, the animals are typically transfected with the reporter gene in a viral promoter.² This mechanism has been adopted for gene expression, drug discovery and gene therapy *etc.*³ Bioluminescence tomography (BLT) has emerged as a valuable imaging technique for non-invasively interrogating a living small animal models. With BLT, 3-D localization is enabled of a bioluminescence source distribution. Comparing to other optical modality such as fluorescence tomography (FMT), bioluminescence tomography has a high sensitivity with a low signal to background ratio. Therefore, BLT is particularly attractive for *in vivo* applications.

In bioluminescence tomography experiments, the light is emitted when luciferin is combined with luciferase in the presence of oxygen and ATP, and luciferase enzymes are generally from firefly (FLuc), click beetle (CBGr68, CBRed), and Renilla reniformis (HRLuc).⁴ So signal has different emission spectra, roughly from 400nm to 750nm, which can be detected by a cooled charge-coupled device (CCD) camera. Bioluminescent signal measured on the surface of the small animal forms the basis for BLT reconstruction. However, the unavailability of external illumination sources, three-dimensional (3D) bioluminescent reconstruction from boundary data is not unique

Further author information: (Send correspondence to Kebin Jia and Jie Tian)

Kebin Jia: E-mail: kebjn@bjut.edu.cn, Telephone: +86 (10)-67396150

Jie Tian: E-mail: tian@ieee.org, Telephone: +86 (10)-82628760

and a highly ill-posed inverse problem in the general case.⁵ Therefore, there is a great impetus for localizing bioluminescent sources uniquely and accurately.^{1,5} At the same time, the development of a fast and robust tomographic algorithm are topics for further investigation.^{1,6}

The uniqueness research of BLT shows that *a priori* information has a quite effect on source reconstruction,⁵ it is essential to incorporate sufficient *a priori* information to get a physically favorable solution. In bioluminescent experiments, bioluminescent photons emitted at 400nm - 700nm undergo less attenuation, as a consequence, the spectrum of the bioluminescent source observed on the surface will be modified depending on the depth of the emission site in tissue. Thus, hyperspectral or multispectral data is expected to reduce the ill-posedness of the inverse problem and improve reconstruction quality.⁷ Recently, the importance of the spectral characteristic of bioluminescent source which can be used as *a priori* information to improve BLT reconstruction has been realized. Noted that multispectral data acquisition could enhance the reconstruction result, dimensional disaster also arises from multispectral measurement and the large-scale data set seriously affects the reconstruction speed,⁸ so there is an increasing interest in multispectral bioluminescence tomography.^{6,7,9-15}

In this paper, a fast tomographic reconstruction algorithm for BLT is proposed and developed. Based on the diffusion approximation model, adaptive finite element algorithm is employed to reconstruct the underlying source distribution. Then the linear relationship between the measured data and unknown source is established through the optimal permissible source region strategy.¹⁴ The use of optimal permissible source region strategy not only reduces the ill-posedness of BLT but also avoids the dimensional disaster arising from the utility of multispectral data. Furthermore, singular value decomposition analysis is presented for data dimensionality reduction and improving computational efficiency in the algorithm. Finally, numerical simulations show the effectiveness of the tomographic algorithm with a heterogenous phantom.

2. METHODS

2.1 Forward model

In bioluminescence tomography, the propagation of photon migration in biological tissues can be well modelled by the steady-state diffusion equation and Robin boundary condition.¹⁶ Taking the influence of light wavelength λ on tissue optical property into account, the following equations are given:

$$-\nabla \cdot (D(\mathbf{x}, \lambda) \nabla \Phi(\mathbf{x}, \lambda)) + \mu_a(\mathbf{x}, \lambda) \Phi(\mathbf{x}, \lambda) = S(\mathbf{x}, \lambda) \quad (\mathbf{x} \in \Omega) \quad (1)$$

$$\Phi(\mathbf{x}, \lambda) + 2A(\mathbf{x}; n, n') D(\mathbf{x}, \lambda) (\mathbf{v}(\mathbf{x}) \cdot \nabla \Phi(\mathbf{x}, \lambda)) = 0 \quad (\mathbf{x} \in \partial\Omega) \quad (2)$$

where Ω is a bounded smooth domain in the three-dimensional Euclidean space R^3 that contains an object to be imaged; $\partial\Omega$ is the corresponding boundary; $\Phi(\mathbf{x}, \lambda)$ denotes the photon flux density [$Watts/mm^2$]; $S(\mathbf{x}, \lambda)$ is the bioluminescent source density [$Watts/mm^3$]; $\mu_a(\mathbf{x}, \lambda)$ is the absorption coefficient [mm^{-1}]; $D(\mathbf{x}, \lambda) = 1/(3(\mu_a(\mathbf{x}, \lambda) + (1-g)\mu_s(\mathbf{x}, \lambda)))$ is the optical diffusion coefficient, $\mu_s(\mathbf{x}, \lambda)$ the scattering coefficient [mm^{-1}], and g the anisotropy parameter; $\nu(\mathbf{x})$ the unit outer normal on $\partial\Omega$. Given the mismatch between the refractive indices n for Ω and n' for the external medium, $A(\mathbf{x}; n, n')$ can be approximately represented:

$$A(\mathbf{x}; n, n') \approx \frac{1 + R(\mathbf{x})}{1 - R(\mathbf{x})} \quad (3)$$

where n' is close to 1.0 when the mouse is in air; $R(\mathbf{x})$ can be approximated by $R(\mathbf{x}) \approx -1.4399n^{-2} + 0.7099n^{-1} + 0.6681 + 0.0636n$.¹⁷ The measured quantity is the outgoing flux density $Q(\mathbf{x}, \lambda)$ on $\partial\Omega$, that is:

$$Q(\mathbf{x}, \lambda) = -D(\mathbf{x}, \lambda) (\mathbf{v}(\mathbf{x}) \cdot \nabla \Phi(\mathbf{x}, \lambda)) = \frac{\Phi(\mathbf{x}, \lambda)}{2A(\mathbf{x}; n, n')} \quad (\mathbf{x} \in \partial\Omega) \quad (4)$$

2.2 Reconstruction method

In the practical experiment, the outgoing flux density can be detected using the filter of bandpass. Therefore, the spectrum can be divided into certain numbers of bands $\tau_l \in [\lambda_l, \lambda_{l+1}], l = 1, 2, \dots, m$. Based on the finite element theory,¹⁸ the weak solution of flux density $\Phi(\mathbf{x}, \tau_l) \in H^1(\Omega)$ on each band τ_l is given through the Eqs. (1) and (2):

$$\begin{aligned} & \int_{\Omega} (D(\mathbf{x}, \tau_l)(\nabla \Phi(\mathbf{x}, \tau_l)) \cdot (\nabla \Psi(\mathbf{x}, \tau_l)) + \mu_a(\mathbf{x}, \tau_l)\Phi(\mathbf{x}, \tau_l)\Psi(\mathbf{x}, \tau_l))d\mathbf{x} \\ & + \int_{\partial\Omega} \frac{1}{2A(\mathbf{x}; n, n')} \Phi(\mathbf{x}, \tau_l)\Psi(\mathbf{x}, \tau_l)d\mathbf{x} = \int_{\Omega} S(\mathbf{x}, \tau_l)\Psi(\mathbf{x}, \tau_l)d\mathbf{x} \quad (\forall \Psi(\mathbf{x}, \tau_l) \in H^1(\Omega)) \end{aligned} \quad (5)$$

In the framework of adaptive finite element analysis, let $\{T_1, \dots, T_k, \dots\}$ be a sequence of nested triangulation of the given domain Ω based on adaptive mesh refinement, where the sequence gradually changes from coarse to fine along with the increase in k .¹⁹ Now, we only consider the k th discretized level which includes N_{T_k} elements and P_k surface measurement points. Then we assemble over all the elements by the finite element method, the matrix form of Equ. (5) are obtained on the single-band τ_l :

$$(K_k(\tau_l) + C_k(\tau_l) + B_k(\tau_l))\Phi_k(\tau_l) = F_k(\tau_l)S_k(\tau_l) \quad (6)$$

where the components of the above matrices $K_k(\tau_l)$, $C_k(\tau_l)$, $B_k(\tau_l)$, $F_k(\tau_l)$ are given:

$$\left\{ \begin{array}{l} k_{ij}^k(\tau_l) = \int_{\Omega} D(\mathbf{x}, \tau_l)(\nabla \psi_i^k(\mathbf{x}, \tau_l)) \cdot (\nabla \psi_j^k(\mathbf{x}, \tau_l))d\mathbf{x} \\ c_{ij}^k(\tau_l) = \int_{\Omega} \mu_a(\mathbf{x}, \tau_l)\psi_i^k(\mathbf{x}, \tau_l)\psi_j^k(\mathbf{x}, \tau_l)d\mathbf{x} \\ b_{ij}^k(\tau_l) = \int_{\partial\Omega} \psi_i^k(\mathbf{x}, \tau_l)\psi_j^k(\mathbf{x}, \tau_l)/(2A(\mathbf{x}; n, n'))d\mathbf{x} \\ f_{ij}^k(\tau_l) = \int_{\Omega} \psi_i^k(\mathbf{x}, \tau_l)\psi_j^k(\mathbf{x}, \tau_l)d\mathbf{x} \end{array} \right. \quad (7)$$

Let $M_k(\tau_l) = K_k(\tau_l) + C_k(\tau_l) + B_k(\tau_l)$, in view to $M_k(\tau_l)$ is a sparse positive definite matrix, we have:

$$\Phi_k(\tau_l) = M_k^{-1}(\tau_l)F_k(\tau_l)S_k(\tau_l) \quad (8)$$

By removing those rows of $[M_k^{-1}(\tau_l)F_k(\tau_l)]$ corresponding to nonmeasurable points,¹⁶ we obtain:

$$\Phi_k(\tau_l) = A_k(\tau_l)S_k(\tau_l) \quad (9)$$

Commonly, the energy contribution of each spectral band τ_l can be determined by performing a beforehand spectral analysis, that is $S(\tau_l) = \omega(\tau_l) \cdot S$, where $\omega(\tau_l) \geq 0$ and $\sum_{l=1}^m \omega(\tau_l) \approx 1$, S denotes the total photon density. At the coarsest level ($k = 1$), the whole reconstruction object Ω is assumed to be the permissible source solution S_1 , taking into account the above spectral distribution, based on Equ. (9), we obtain:

$$A^T AS_1 = A^T \Phi \quad (10)$$

Where

$$A = \begin{bmatrix} \omega(\tau_1)A_1(\tau_1) \\ \omega(\tau_2)A_1(\tau_2) \\ \vdots \\ \omega(\tau_m)A_1(\tau_m) \end{bmatrix}, \Phi = \begin{bmatrix} \Phi_1(\tau_1) \\ \Phi_1(\tau_2) \\ \vdots \\ \Phi_1(\tau_m) \end{bmatrix}$$

A^T is the transpose of A and $A^T \cdot A$ is an $mN_{T_1} \times mN_{T_1}$ symmetric matrix, then Equ. (10) has become a standard linear equation. Given the initial guess S_1^0 of S_1 , the solution S_1 can be updated iteratively by:

$$S_1^{n+1} = S_1^n + \alpha_n \beta_n \quad (11)$$

Where n is iteration number, β_n is the searching direction,

$$\beta_n = A^T AS_1^n - A^T \Phi \quad (12)$$

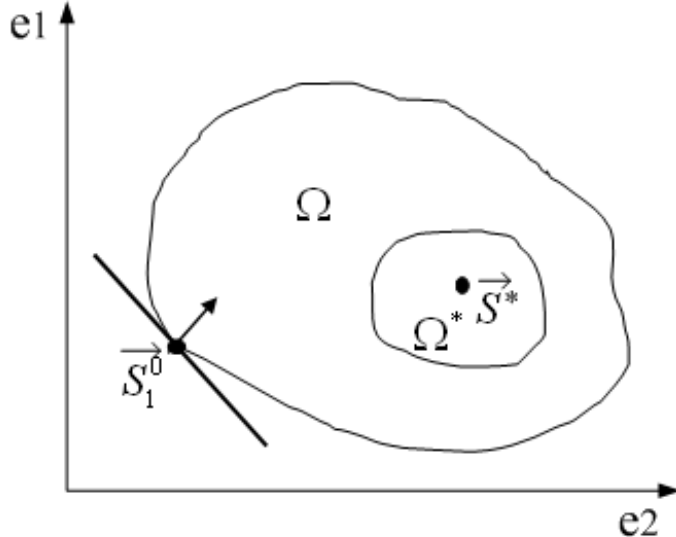


Figure 1. The sketch of searching optimal permissible source region.

α_n is the step size,

$$\alpha_n = \frac{\|\beta_n\|}{\|A \cdot \beta_n\|} \quad (13)$$

In the iteration process, we directly use the measured data $\Phi_1^{meas}(\tau_l)$ to substitute $\Phi_1(\tau_l)$, because the effect of noise is low originally. When $\|\beta_n\| \leq \delta$ or iteration number $n > N_{max}$, the iteration is terminated and the rough region of the optimal solution S^* is obtained, that is Ω^* . We name it the optimal permissible source region and the sketch is shown in Fig. 1. Otherwise, S_1 is updated by Equ. (11).

In BLT, taking into account the real physical meaning, the source density constrain can be taken as *a priori* information. Therefore, the nonnegative penalty is adopted during the iteration process.

Reformulate Equ. (8): $\Phi_k(\tau_l) = M_k^{-1}(\tau_l)F_k(\tau_l)S_k(\tau_l)$, taking into account the linear relation between the unknown source value S_k and boundary measured points Φ_k^{meas} , we have:

$$\Phi_k^{meas}(\tau_l) = G_k(\tau_l)S_k(\tau_l) \quad (14)$$

Where $G_k(\tau_l)$ can be established by deleting the rows of $[M_k^{-1}(\tau_l)F_k(\tau_l)]$ corresponding to unmeasured points. Incorporating the optimal permissible source region, we have:

$$\Phi_k^{meas}(\tau_l) = G_k(\tau_l)W_k(\tau_l)S_k(\tau_l) \quad (15)$$

And $W_k(\tau_l)$ is a diagonal matrix for selecting the permissible region, that is:

$$W_k(\tau_l) = Diag(w_{k(11)}, w_{k(22)}, \dots, w_{k(ii)}, \dots, w_{k(N_{P_l}N_{P_l})})$$

$$w_{k(ii)} = \begin{cases} 1 & \{s_{k(i)} \geq \gamma^k s_k^{max}\} \\ 0 & \{s_{k(i)} < \gamma^k s_k^{max}\} \end{cases}$$

When $k = 1$, $s_{k(i)}$ is the optimal solution S^* and s_k^{max} is its maximum. $k \geq 2$, $s_{k(i)}$ and s_k^{max} are the reconstructed results prolonged from $(k-1)$ th level and the corresponding maximum, that is

$$S_k = I_{k-1}^k S_{k-1} \quad (k \geq 2) \quad (16)$$

S_{k-1} is the reconstruction result on $(k-1)$ th level and γ^k is the ratio factor. By retaining the columns of $[G_k(\tau_l)W_k(\tau_l)]$ corresponding to the permissible region S_k^p , the final form of the linear system between the measurable boundary flux $\Phi_k^{meas}(\tau_l)$ and S_k^p is obtained:

$$A_k(\tau_l)S_k^p = \Phi_k^{meas}(\tau_l) \quad (17)$$

In order to enhance computational efficiency, singular value decomposition was adopted to reduce dimensional disaster.⁷ We organized the boundary measurement of different band as a matrix Φ^{meas} :

$$\Phi^{meas} = [\Phi_k^{meas}(\tau_1) \quad \Phi_k^{meas}(\tau_2) \quad \dots \quad \Phi_k^{meas}(\tau_m)]^T \quad \Phi^{meas} \in \mathbb{R}^{m \times P_k} \quad (18)$$

A SVD of matrix Φ^{meas} yielded the principal spectral basis vectors \mathbf{u}_i and the principal depth contributing vectors \mathbf{v}_i i.e. $\Phi^{meas} = \sum_i^P \sigma_i \mathbf{u}_i \mathbf{v}_i$. We then constructed a reduced-dimension subspace from the t left singular vectors corresponding the set of singular values that constitute more than 95% of the energy. The t left singular vectors $\mathbf{U} = [\mathbf{u}_1 \quad \mathbf{u}_2 \quad \dots \quad \mathbf{u}_t]^T, \mathbf{U} \in \mathbb{R}^{m \times t}$. Each principal basis vector is a function of wavelength τ_l as

$$u_i = [u_j(\tau_1) \quad u_j(\tau_2) \quad \dots \quad u_j(\tau_m)]^T, u_j \in \mathbb{R}^m, j = 1, 2, \dots, t \quad (19)$$

By projecting the measurements and the forward model onto the j th spectral basis vector, we obtain:

$$\tilde{b}_j = \tilde{A}_j S_k^p \quad (20)$$

where

$$\tilde{b}_j = \sum_i^m \Phi_k^{meas}(\tau_i) u_j(\tau_i), \quad \tilde{A}_j = \sum_i^m \omega(\tau_i) u_j(\tau_i) A_k(\tau_i) \quad (21)$$

In the multispectral case, the linear system can be obtained:

$$b_k^{mul} = A_k^{mul} S_k^p \quad (22)$$

where

$$b_k^{mul} = [\tilde{b}_1 \quad \tilde{b}_2 \quad \dots \quad \tilde{b}_t] \quad b_k^{mul} \in \mathbb{R}^{mt}$$

$$A_k^{mul} = [\tilde{A}_1^T \quad \tilde{A}_2^T \quad \dots \quad \tilde{A}_t^T] \quad A_k^{mul} \in \mathbb{R}^{mt \times P_k}$$

Finally, the k th objective function was established:

$$\min_{S_{inf}^k \leq S_k^p \leq S_{sup}^k} \Theta_k(S_k^p) = \{\|A_k^{mul} S_k^p - b_k^{mul}\|_\Lambda + \sigma_k \cdot (S_k^p - S_k^{init})^T (S_k^p - S_k^{init})\} \quad (23)$$

where s_{inf}^k and s_{sup}^k are the k th level lower and upper bounds of the source density; Λ is the weight matrix, $\|\Lambda\|_\Lambda = V^T \Lambda V$; σ_k the regularization parameter. S_k^{init} is initial value at the k th level. And a spectral projected gradient-based large-scale optimization algorithm is modified to solve the least square problem.^{20–22}

3. RESULTS

In order to evaluate our approach, a heterogeneous phantom of 30mm height and 10mm radius is designed. It was made up of four ellipsoids and one cylinder to represent muscle (M), lungs (L), heart (H), bone (B) and Liver (Li), as shown in Fig. 2(a). Taking into account *inverse crime*, a virtual optical environment (MOSE) is employed to produce the synthetic data which is developed to simulate the photon transportation based on Monte Carlo Method.²³ The discretized mesh used in MOSE illustrated in Fig. 2(b) has a maximum element diameter

Table 1. Optical property parameters in different wavelength range (Unit: mm^{-1}).

Wavelength	500 – 550nm		550 – 600nm		600 – 650nm		650 – 700nm		700 – 750nm	
	μ_a	μ_s'								
Muscle	$6.2e-4$	1.34	$2.5e-4$	1.28	$2.1e-4$	1.22	$3.4e-4$	1.18	$1.2e-3$	1.14
Lung	$2.7e-2$	2.41	$7.1e-3$	2.30	$2.0e-3$	2.21	$1.4e-3$	2.12	$2.8e-3$	2.04
Bone	$9.0e-3$	3.34	$2.2e-3$	2.93	$6.0e-4$	2.61	$3.6e-4$	2.34	$5.9e-4$	2.21
Heart	$9.1e-3$	1.28	$2.2e-3$	1.13	$6.9e-4$	1.00	$5.8e-4$	0.91	$1.4e-3$	0.82
Liver	$5.4e-2$	0.83	$1.2e-2$	0.76	$3.4e-3$	0.70	$2.0e-3$	0.65	$3.0e-3$	0.60

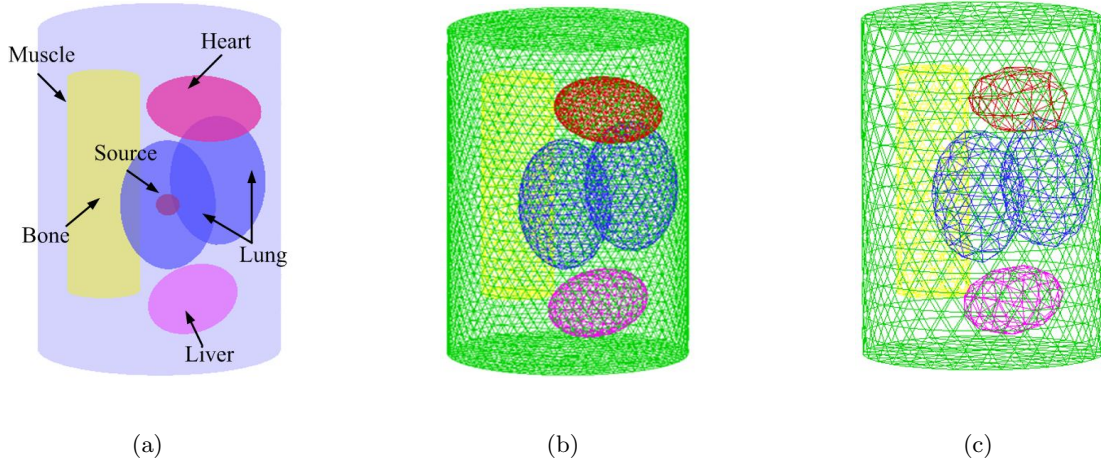


Figure 2. Heterogeneous phantom. (a) The heterogeneous phantom with Muscle, Bone, Heart, Lungs, Liver and a single source in the lung; (b) The discretized mesh used in MOSE; (c) The mesh used in reconstruction algorithm.

of 1mm. In the experiment, the solid spherical source with 1mm radius had source power of 1 nano-Watts and was put at (-3, 5, 15) inside the right lung as shown in Fig. 2(a). The initial coarser mesh used in reconstruction algorithm was demonstrated in Fig. 2(c) with the maximal element diameter of 2mm. Based on the emission spectral distribution, the spectrum [500nm ~ 700nm] can be divided into five discrete bins with steps of 50nm. In the experiments, the optical properties of each component are assumed as *a priori* information and optical property parameters of each bin are compiled in Table 1.⁶

In the reconstruction process, in order to compare with our algorithm, several reconstruction algorithms were performed in the same data set and computation environment which was Pentium 4 2.8 GHz and 760 MB RAM. First, the reconstruction algorithm (Tradition) without optimal permissible source region nor SVD was carried out as shown in Fig. 3(a). Figure 3(b) demonstrates the reconstruction result using the method (Optimal) only with the optimal permissible source region strategy. Finally, with the proposed algorithm, the reconstructed result was shown in Fig. 3(c). Quantitative comparisons were compiled in Table 2. The comparison results reveals the method's capabilities for fast localizing the bioluminescent source accurately.

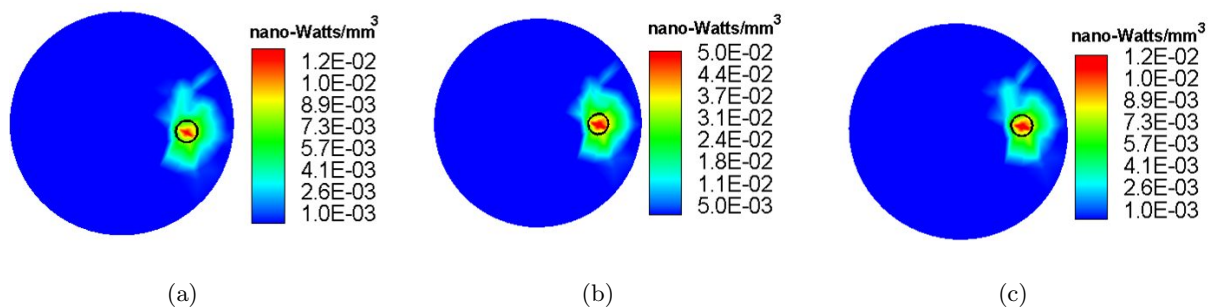


Figure 3. Reconstruction results. (a) The result with traditional method; (b) The result only with optimal permissible source region; (c) The reconstructed result with proposed algorithm. The cross section perpendicular to z-axis direction is through the actual source's center. The black circle denotes the actual source positions.

Table 2. Quantitative comparisons between different methods

Methods	Actual position	Reconstructed position	Reconstructed time (hours)
Tradition	(-3, 5, 15)	(-2.96, 5.43, 15.81)	12
Optimal	(-3, 5, 15)	(-2.96, 5.44, 15.82)	0.67
Proposed	(-3, 5, 15)	(-2.96, 5.44, 15.82)	0.5

4. CONCLUSIONS

Multispectral BLT is becoming new research hot spot and facing many challenges such as the ill-posedness of BLT and computational burden. In the paper, an optimal permissible source region strategy is developed to reduce ill-posedness of BLT and a singular value analysis is adopted to enhance computational efficiency. The reconstruction method can realize the preferable localization of bioluminescent source along with the reduction of time and memory cost. In this paper, using the proposed BLT algorithm, the localization of bioluminescent source is preferred. The ill-posedness of BLT is not only reduced, but also the computational efficiency is improved. The future work is to further verify the proposed algorithm with the physical BLT experiment and the corresponding results will be reported later.

ACKNOWLEDGMENTS

This work is supported by the National Natural Science Foundation of China under Grant No. 60672050, 30672690, 30600151, 90209008, 60532050, 60621001, 30873462 and Funding Project for Academic Human Resources Development (PHR) under Grant No. 00627, the Project for the National Basic Research Program of China (973) under Grant No. 2006CB705700, Changjiang Scholars and Innovative Research Team in University (PCSIRT) under Grant No.IRT0645, CAS Hundred Talents Program, CAS scientific research equipment develop program (YZ0642, YZ200766), 863 Program under Grant No. 2006AA04Z216, the Joint Research Fund for Overseas Chinese Young Scholars under Grant No. 30528027, Beijing Natural Science Fund under Grant No. 4071003.

REFERENCES

1. V. Ntziachristos, J. Ripoll, L. V. Wang, and R. Weissleder, "Looking and listening to light: the evolution of whole-body photonic imaging," *Nat. Biotech.* **23**, pp. 313–320, 2005.
2. W. Cong, D. Kumar, Y. Liu, A. Cong, and G. Wang, "A practical method to determine the light source distribution in bioluminescent imaging," *Proc. SPIE* **5535**, pp. 679–686, 2004.
3. T. F. Massoud and S. S. Gambhir, "Molecular imaging in living subjects: seeing fundamental biological processes in a new light," *Genes Dev.* **17**, pp. 545–580, 2003.
4. H. Zhao, T. C. Doyle, O. Coquoz, F. Kalish, B. W. Rice, and C. H. Contag, "Emission spectra of bioluminescent reporters and interaction with mammalian tissue determine the sensitivity of detection *in vivo*," *J. Biomed. Opt.* **10**, pp. 041210–1–9, 2007.
5. G. Wang, Y. Li, and M. Jiang, "Uniqueness theorems in bioluminescence tomography," *Med. Phys.* **31**, pp. 2289–2299, 2004.
6. Y. Lv, J. Tian, W. Cong, G. Wang, W. Yang, C. Qin, and M. Xu, "Spectrally resolved bioluminescence tomography with adaptive finite element analysis: methodology and simulation," *Phys. Med. Biol.* **52**, pp. 4497–4512, 2007.
7. A. J. Chaudhari, F. Darvas, J. R. Bading, R. A. Moats, P. S. Conti, D. J. Smith, S. R. Cherry, and R. M. Leahy, "Hyperspectral and multispectral bioluminescence optical tomography for small animal imaging," *Phys. Med. Biol.* **50**, pp. 5421–5441, 2005.
8. S. Ahn, A. J. Chaudhari, F. Darvas, C. A. Bouman, and R. M. Leahy, "Fast iterative image reconstruction methods for fully 3d multispectral bioluminescence tomography," *Phys. Med. Biol.* **53**, pp. 3921–3942, 2008.
9. W. Han, W. Cong, and G. Wang, "Mathematical study and numerical simulation of multispectral bioluminescence tomography," *International Journal of Biomedical Imaging* **2006**, pp. 1–15, 2006.
10. O. Coquoz, T. L. Troy, D. Jekic-McMullen, and B. W. Rice, "Determination of depth of *in vivo* bioluminescent signals using spectral imaging techniques," *Proc. SPIE* **4967**, pp. 1605–7422, 2003.
11. G. Alexandrakis, F. R. Rannou, and A. F. Chatzioannou, "Tomographic bioluminescence imaging by use of a combined optical (opt) system: a computer simulation feasibility study," *Phys. Med. Biol.* **50**, pp. 4225–4241, 2005.
12. A. X. Cong and G. Wang, "Multispectral bioluminescence tomography: methodology and simulation," *International Journal of Biomedical Imaging* **2006**, pp. 1–7, 2006.

13. H. Dehghani, S. C. Davis, S. Jiang, B. W. Pogue, K. D. Paulsen, and M. S. Patterson, "Spectrally resolved bioluminescence optical tomography," *Optics Letters* **31**, pp. 365–367, 2006.
14. J. Feng, K. Jia, G. Yan, S. Zhu, C. Qin, Y. Lv, and J. Tian, "An optical permissible source region strategy for multispectral bioluminescence tomography," *Optics Express* **16**, pp. 15640–15654, 2008.
15. J. Tian, J. Bai, X. Yan, S. Bao, Y. Li, W. Liang, and X. Yang, "Multimodality molecular imaging," *IEEE EMB Magazine* **27**, pp. 48–57, 2008.
16. W. Cong, G. Wang, D. Kumar, Y. Liu, M. Jiang, L. V. Wang, E. A. Hoffman, and G. McLennan, "Practical reconstruction method for bioluminescence tomography," *Optics Express* **13**, pp. 6756–6671, 2005.
17. M. Schweiger, S. R. Arridge, M. Hiraoka, and D. T. Delpy, "The finite element method for the propagation of light in scattering media: Boundary and source conditions," *Med. Phys.* **22**, pp. 1779–1792, 1995.
18. S. S. Rao, *The finite element method in engineering*, Butterworth-Heinemann, Boston, 1999.
19. Y. Lv, J. Tian, W. Cong, G. Wang, J. Luo, W. Yang, and H. Li, "A multilevel adaptive finite element algorithm for bioluminescence tomography," *Optics Express* **14**, pp. 8211–8223, 2006.
20. P. E. Gill, W. Murray, and M. Wright, *Practical optimization*, Academic Press, New York, 1981.
21. E. G. Birgin and J. M. Martinez, "A box-constrained optimization algorithm with negative curvature directions and spectral projected gradients," *Computing* **15**, pp. 49–60, 2001.
22. E. G. Birgin and J. M. Martinez, "Large-scale active-set box-constrained optimization method with spectral projected gradients," *Comput. Optim. Appl.* **23**, pp. 101–125, 2002.
23. H. Li, J. Tian, F. Zhu, W. Cong, L. V. Wang, E. A. Hoffman, and G. Wang, "A mouse optical simulation environment (mose) to investigate bioluminescent phenomena in the living mouse with the monte carlo method," *Acad. Radiol.* **11**, pp. 1029–1038, 2004.